A NUMERICAL INVESTIGATION ON THE UNSTABLE FLOW IN A SINGLE STAGE OF AN AXIAL COMPRESSOR

B. Farhanieh, N. Amanifard and K. Ghorbanian

Thermo-Fluids Department, School of Mechanical Engineering, Sharif University of Technology
Tehran, Iran, bifa@sina.sharif.ac.ir - namanifard@hotmail.com - Kaveh@sina.sharif.ac.ir

(Received: April 9, 2002 - Accepted in Revised Form: May 15, 2003)

Abstract An unsteady two-dimensional finite-volume solver was developed based on Van Leer's flux splitting algorithm in conjunction with "Monotonic Upstream Scheme for Conservation Laws (MUSCL)" limiters to improve the order of accuracy and the two-layer Baldwin-Lomax turbulence model was also implemented. Two test cases were prepared to validate the solver. The computed results were compared with the experimental data and a good agreement validated the solver. Finally, the solver was used for the flow through a multi-blade stage of an axial compressor in its off-design condition. The computed results showed a rotating stall-like instability with a periodic behavior. To investigate the flow properties during the instability condition, the flow pattern, Vortex properties and the axial velocity were studied. It was concluded that the instability vortices in the multi-blade cascade do not have the same generation history of the separated vortices over a single body.

Key Words Flow Instability, Cascade Study, Finite-Volume, Axial Compressors

چکیده یک کد کامپیوتری حل معادلات جریان لزج دو بعدی به روش حجم های محدود آماده شد و در آن روش تفکیک شار Van- Leer برای محاسبه عددی شارهای ممنتم به کار گرفته شد. همچنین به منظور جلوگیری از نوسانات عددی و افزایش دقت محاسبات محدود کننده Van-Leer از خانواده بالا دست یکنواخت برای قانون محافظه کار (MUSCL) مورد استفاده قرار گرفت و مدل توربولانس دو لایه Baldwin-Lomax (BL) در رژیم آشفته بکار گرفته شد. برا ی تا ییید صحت عملکرد کد، دو مساله نمونه حل شد و نتایج انطباق خوبی با داده های آزمایشگاهی داشت. سپس مساله جریان ناپایدار در یک طبقه از یک کمپرسور محوری مورد حل قرار گرفت. نتایج ناپایداری از گونه سکته دورانی را نشان داد که دارای رفتاری نوسانی است. برای این حالت خواص و الگوی جریان در زمان های معین مطالعه شد و ویژگیهای گرداب های جریان ناپایدار به طور ویژه مطالعه شد. نتایج بیان می‌دارد که حرکت و توسعه گردابهای ناپایداری در یک کسکید کاملا" با وضعیت گرابهای پشت یک هوابر در جریانی با زاویه حمله زیاد متفاوت است. می‌توان دریافت که عواملی مثل هندسه چند پره ای و کاهش دبی جرمی و گرادیان فشار مثبت با عث آغاز چنین گردابه هایی گردیده است.

1. INTRODUCTION

The analysis of the flow field in unstable condition, especially in Gas-Turbine engines, has mainly been based on experimental observations and studies during last decay [1-3]. Recently, several computational fluid dynamics (CFD) codes have been developed. The axial compressors with their adverse pressure gradients in through flow direction, are the most critical component in Gas-Turbine engines from the viewpoint of flow instability phenomena. Today, the use of CFD tools is a standard practice in the study of the cascade flow within the stable operating range of a compressor. However, the CFD approach still needs to be developed as a sound prediction method for operation in the unstable region. Studies of Sisto et al. [4] and Jonnavithula et al. [5] have resulted in notable progress in use of CFD-type techniques for the calculation of instability effects. They used a two-dimensional discrete vortex model with the separation point being obtained by an integral boundary layer. The evolution of stall is well predicted when compared with their experiment, although only up to six blade passages were used in the computation. Further, He [6] carried out a numerical study in a single stage of an axial compressor. The Navier-Stokes equations were discretized in space by finite volume method and integrated in time by

using a four-stage Rung-Kutta scheme. The second- and fourth-order blended smoothing was adopted in both the stream wise and circumferential directions for numerical damping, and Baldwin-Lomax turbulence model was also adopted. Outa et al. [7], made a numerical simulation for stall cells in rotor-stator frame of a compressor, using viscous approach. Furthermore, Saxer et al. [8] carried out a numerical study for inviscid flow passing through axial compressors, and the history of stall vortices were investigated for a fifteen-blade passage of a single stage. The mass flow rate fluctuations were approximately similar to those obtained from their experimental observations.

The scope of this work is twofold. First, to introduce and validate a two-dimensional density-based flow equations solver, and second, preparing a numerical study on rotating stall inception using a viscous approach in a stage of an axial compressor studies.

In the present work, the computational test cases have been carried out to validate the solver and to study the implementation of flux splitting methods with MUSCL limiters in a multi-block computational domain, with the modified Baldwin-Lomax turbulent model.

2. GOVERNING EQUATIONS

For a given thermodynamic system having two intensive degree of freedom, its fluid dynamic behaviour can generally be described by means of the system of conservation laws corresponding to the conservation of total mass, momentum and energy.

Let Q be an unknown vector defined for a two-dimensional study as follows:

$$\mathbf{Q}=[\rho,\rho u,\rho v,\rho E]^T=[q_1,q_2,q_3,q_4]^T \quad (1)$$

where E is the total energy ($E = e + (u^2 + v^2)/2$). Let V be any volume with bounding surface ∂V and outward unit normal **n.** Assuming that the volume does not vary with time, **Q** satisfies the following integral conservation law:

$$\frac{d}{dt}\int_V \mathbf{Q}\,dV=\int_V \frac{\partial}{\partial t}\mathbf{Q}\,dV = -\oint_{\partial V} \mathbf{F}\cdot\mathbf{n}\,dS \quad (2)$$

The equivalent differential form of Equation 2, in an inertial reference system reads:

$$\frac{\partial}{\partial t}\mathbf{Q} = -\nabla\cdot\mathbf{F} \quad (3)$$

This accounts for the inviscid ($\mathbf{F_E}$) and viscous ($\mathbf{F_V}$) contributions, i.e.

$$\mathbf{F} = \mathbf{F}_E - \mathbf{F}_V \quad (4)$$

where

$$\mathbf{F}_E = [\rho\,\mathbf{u},\ \rho\,\mathbf{uu} + p\mathbf{I},\ \rho\,\mathbf{u}\boldsymbol{H}]^T \quad (5\text{-a})$$

$$\mathbf{F}_V = [0,\ \sigma,\ -(\mathbf{q} - \mathbf{u}\cdot\sigma)]^T \quad (5\text{-b})$$

For an ideal gas the pressure is related to the density and temperature according to the equation of state;

$$p = \rho RT \quad (6)$$

The stress tensor and heat flux is determined according to the Newton's and Fourier's laws by:

$$\sigma = \mu(\nabla\mathbf{u} + \nabla\mathbf{u}^T) - \frac{2}{3}\mu\nabla\cdot\mathbf{u}\mathbf{I} \quad (7)$$

$$\mathbf{q} = -\lambda\nabla T \quad (8)$$

From kinetic theory it can be shown that, for a thermodynamic system having only two intensive degree of freedom, the viscousity (μ) and the heat conduction (λ) coefficients depend only upon the gas temperature.

The conservation equations are formally closed once the rate of all fluxes on the boundary ∂V and the initial state of **Q** are known. However, the determination of the boundary fluxes and the mathematical closure is not yet resolved [9]. Moreover, the numerical treatment of the boundary conditions is a very critical issue that requires a detailed analysis.

The governing equations transforms to a computaional coordinate for the numerical solution. The transformed equations in general

computational domain reads:

$$\frac{\partial \overline{\mathbf{Q}}}{\partial \tau}+\frac{\partial \overline{\mathbf{E}}}{\partial \xi}+\frac{\partial \overline{\mathbf{F}}}{\partial \eta}=\frac{\partial \overline{\mathbf{E}}_v}{\partial \xi}+\frac{\partial \overline{\mathbf{F}}_v}{\partial \eta} \tag{9}$$

The parameters in Equation 9, are related to physical vectors with following general relations:

$$\overline{\mathbf{Q}}=\frac{\mathbf{Q}}{J} \tag{10-a}$$

$$\overline{\mathbf{E}}=\frac{1}{J}(\xi_x \mathbf{F}_{Ex}+\xi_y \mathbf{F}_{Ey}) \tag{10-b}$$

$$\overline{\mathbf{F}}=\frac{1}{J}(\eta_x \mathbf{F}_{Ex}+\eta_y \mathbf{F}_{Ey}) \tag{10-c}$$

$$\overline{\mathbf{E}_v}=\frac{1}{J}(\xi_x \mathbf{F}_{vx}+\xi_y \mathbf{F}_{vy}) \tag{10-d}$$

$$\overline{\mathbf{F}_v}=\frac{1}{J}(\eta_x \mathbf{F}_{vx}+\eta_y \mathbf{F}_{vy}) \tag{10-e}$$

In addition, the following relations can relate the general coordinate to Cartesian coordinate:

$$\tau=(t,x,y) \tag{11-a}$$

$$\xi=(t,x,y) \tag{11-b}$$

$$\eta=(t,x,y) \tag{11-c}$$

$$\xi_x=Jy_\eta \tag{12-a}$$

$$\xi_y=-Jx_\eta \tag{12-b}$$

$$\eta_x=-Jy_\xi \tag{12-c}$$

$$\eta_y=Jx_\xi \tag{12-d}$$

where:

$$J=\frac{1}{x_\xi y_\eta-y_\xi x_\eta}=\frac{\partial(\xi,\eta)}{\partial(x,y)} \tag{13}$$

3. NUMERICAL PROCEDURE

3.1 Finite Volume Formulation Reconsidering Equation 9, the time derivative is approximated by a first-order backward differencing quotient and the remaining terms are evaluated at time level n+1. Thus:

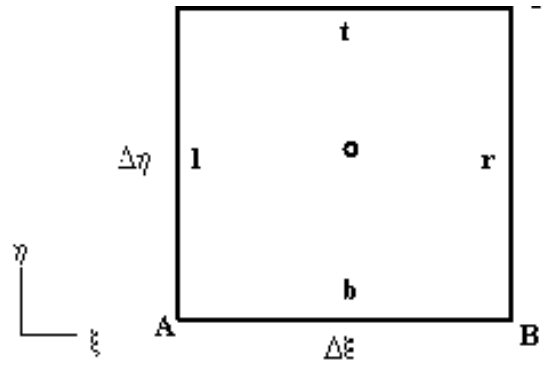

Figure 1. The Finite Volume Cell.

$$\frac{\overline{\mathbf{Q}}^{n+1}-\overline{\mathbf{Q}}^{n}}{\Delta\tau}+(\frac{\partial \overline{\mathbf{E}}}{\partial \xi})^{n+1}+(\frac{\partial \overline{\mathbf{F}}}{\partial \eta})^{n+1}=(\frac{\partial \overline{\mathbf{E}_v}}{\partial \xi})^{n+1}+(\frac{\partial \overline{\mathbf{F}_v}}{\partial \eta})^{n+1} \tag{14}$$

Integrating Equation 14, over square **ABCD** shown in Figure 1, and using Green's Theorem provides:

$$\Delta\overline{\mathbf{Q}}+\frac{\Delta\tau}{\Delta\xi}(\overline{\mathbf{E}}_r-\overline{\mathbf{E}}_l)+\frac{\Delta\tau}{\Delta\eta}(\overline{\mathbf{F}}_t-\overline{\mathbf{F}}_b)=\frac{\Delta\tau}{\Delta\xi}(\overline{\mathbf{E}}_{vr}-\overline{\mathbf{E}}_{vl})+\frac{\Delta\tau}{\Delta\eta}(\overline{\mathbf{F}}_{vt}-\overline{\mathbf{F}}_{vb}) \tag{15}$$

Since, the flux vectors in Equation 15, are evaluated in time step of n+1, by using the Taylor expansion and a first order approximation in time,they can be expressed in terms of $\Delta\overline{\mathbf{Q}}$, and the fux vectors can be evaluated as following:

$$\overline{\mathbf{E}}^{n+1}=\overline{\mathbf{E}}^{n}+\frac{\partial \overline{\mathbf{E}}}{\partial \overline{\mathbf{Q}}}\Delta\overline{\mathbf{Q}}=\overline{\mathbf{E}}^{n}+\mathbf{A}\Delta\overline{\mathbf{Q}} \tag{16-a}$$

$$\overline{\mathbf{F}}^{n+1}=\overline{\mathbf{F}}^{n}+\frac{\partial \overline{\mathbf{F}}}{\partial \overline{\mathbf{Q}}}\Delta\overline{\mathbf{Q}}=\overline{\mathbf{F}}^{n}+\mathbf{B}\Delta\overline{\mathbf{Q}} \tag{16-b}$$

$$\bar{E}_v^{n+1} = \bar{E}_v^{n} + \frac{\partial \bar{E}_v}{\partial \bar{Q}} \Delta \bar{Q} = \bar{E}_v^{n} + A_v \Delta \bar{Q} \quad (16\text{-c})$$

$$\bar{F}_v^{n+1} = \bar{F}_v^{n} + \frac{\partial \bar{F}_v}{\partial \bar{Q}} \Delta \bar{Q} = \bar{F}_v^{n} + B_v \Delta \bar{Q} \quad (16\text{-d})$$

The matrices **A**, **B**, $\mathbf{A}_v$, and $\mathbf{B}_v$ are the Jacobian matrices given by Hoffman et al.[9].

Since, evaluation of inviscid flux vectors on cell faces is the most important problem in numerical solution of Euler and NS equations, the flux splitting methods are discussed in details in the following section. Since the viscous fluxes are related to second derivatives of velocity vectors, they are evaluated by central difference approximation.

3.2 Flux Splitting Hoffman et al. [9] has shown that a hyperbolic equation is unstable for a formulation with central difference approximation. However, the solution would be stable if the governing equation includes a diffusion term. To stabilize the hyperbolic equation approximated by central difference formulation of convective term; the addition of damping terms would be required. Furthermore, the damping terms are used to reduce oscillations within the domain, which may develop near sharp gradients. To avoid the addition of damping terms, the flux vector splitting schemes used to formulate the convective terms and central differencing approximates the diffusion terms.

For a system of equations being classified as hyperbolic, the Jacobian matrix $\mathbf{A}$ must possess real eigenvalues. The eigenvalues of $\mathbf{A}$ represents the charactristic direction of the hyperbolic system and thus provide the direction of the propagation of information. If matrix $\mathbf{A}$ has real eigenvalues and associated eigenvectors, it may be diagonalized; i.e., a similarity transformation exist such that:

$$\mathbf{A} = \mathbf{L}^{-1} \mathbf{\Lambda}_g \mathbf{L} \quad (17)$$

For a Jacobian matrix like A, a large class of flux decomposition can be obtained by defining $A^{\pm}$ as follows:

$$\mathbf{A}^{\pm} = \frac{\mathbf{A} \pm g(\mathbf{A})}{2} \quad (18)$$

and

$$\bar{\mathbf{E}}^{\pm} = \mathbf{A}^{\pm} \bar{\mathbf{Q}} \quad (19)$$

where g(**A**) is:

$$g(\mathbf{A}) = \mathbf{L}^{-1} \mathbf{\Lambda}_g \mathbf{L} \quad (20)$$

and $\mathbf{\Lambda}_g$ is a diagonal matrix whose non-zero coefficients are g_i . These coefficients can be shown with the improper functional notation $g(\lambda_i)$ to indicate the same ordering of λ_i. Thus, the eigenvalues of $\mathbf{A}^{\pm}$ are :

$$\lambda_i^{\pm} = \frac{\lambda_i \pm g(\lambda_i)}{2} \quad (21)$$

Following the current definition, the numerical flux function associated with a flux vector splitting is expressed as:

$$\bar{\mathbf{E}}_r = \bar{\mathbf{E}}^{+}(\bar{\mathbf{Q}}_{i,j}) + \bar{\mathbf{E}}^{-}(\bar{\mathbf{Q}}_{i+1,j}) \quad (22)$$

Similar functions can be defined for other flux vectors at all faces of the finite volume cell.

Van Leer has proposed a splitting method that removes the discontinuous behaviour of the split fluxes by modifying their functional dependence upon the Mach number ***M***. In particular, the split fluxes are represented by a polynomial in ***M*** that gives the same functional values and slope of the unsplit fluxes at ***M*** = ±1. Moreover, the symmetry properties of each split flux component should be the same as those of the unsplit one [10], i.e.

$$\bar{\mathbf{E}}^{+}(\boldsymbol{M}) = \pm \bar{\mathbf{E}}^{-}(\boldsymbol{M}) \text{ if } \bar{\mathbf{E}}(\boldsymbol{M}) = \pm \bar{\mathbf{E}}(-\boldsymbol{M}) \quad (23)$$

The numerical flux function approximating the flux at right face of a finite volume cell shown in Figure 1, is as follows:

$$\bar{\mathbf{E}}_r = \bar{\mathbf{E}}_r^{+}(\bar{\mathbf{Q}}_{i,j}) + \bar{\mathbf{E}}_r^{-}(\bar{\mathbf{Q}}_{i+1,j}) \quad (24)$$

where $\bar{\mathbf{Q}}_{i,j}$ / $\bar{\mathbf{Q}}_{i+1,j}$ is the value of the variable upstream/downstream of the right bounding control surface that represents the left/right state transported by $\bar{\mathbf{E}}_r^{+}$ / $\bar{\mathbf{E}}_r^{-}$.

An extension of the Van Leer-type splitting to multidimensional flows is not quite trivial. The split flux component for two dimwnsional flows can be constructed by retaining the one-dimensional structure. For the present two

dimentional studies, the split flux in physical space is as following [9]:

$$\mathbf{E}_n^{+} = \pm \rho c \frac{(1 \pm \boldsymbol{M}_n)^2}{4} \begin{bmatrix} 1 \\ u \pm (2 - \boldsymbol{M}_n)\frac{c}{k} n_x \\ v \pm (2 - \boldsymbol{M}_n)\frac{c}{k} n_y \\ \frac{c^2}{k-1}(1 + \frac{k-1}{2}\boldsymbol{M}_n^2) \end{bmatrix} \quad (25)$$

3.3 The Van Leer's Limiter To prevent the oscillatory behavior of the numerical results and to increase the accuracy, the Van-Leer's limiter was added to the flux splitting algorithm [10].

Van Leer proposed to cast the polynomial reconstruction in terms of the Legendre polynomial expansion. The method in a compact form is imployed by Farhanieh et.al. [10]. For an unknown variable u the MUSCL can be expressed as:

$$u_l^n = u_i^n + \frac{1}{4}[(1-r)\bar{\delta}^{+} u_{i-1}^n + (1+r)\hat{\delta}^{+} u_i^n] \quad (26)$$

$$u_r^n = u_{i+1}^n - \frac{1}{4}[(1-r)\bar{\delta}^{+} u_{i+1}^n + (1+r)\hat{\delta}^{+} u_i^n] \quad (27)$$

where r =1/3 yields third-order upwind biased scheme and $\hat{\delta}^{+}$ and $\bar{\delta}^{+}$ are the limited slopes:

$$\hat{\delta}^{+} u = \ell(\delta^{+} u_i, \omega\delta^{+} u_{i-1}) \; ; \; \bar{\delta}^{+} u = \ell(\delta^{+} u_i, \omega\delta^{+} u_{i+1}) \quad (28)$$

where $1 \le \omega \ge (3\text{-}r)/(1\text{-}r)$, and ℓ is the Van Leer's minmod limiter function [10]. The simplified form of MUSCL using Van Leer's function becomes:

$$\ell = \frac{2\delta^{-} u . \delta^{+} u}{[(\delta^{-} u)^2 + (\delta^{+} u)^2]}$$
$$f = (1 - r \cdot \ell)\delta^{-} u + (1 + r \cdot \ell)\delta^{+} u \quad (29)$$
$$u_r = u_{i+1,j} - \frac{1}{4} f \cdot \ell$$

It is evident that for other faces the related nodes are used in the same mathematical relations.

3.4 Using the Multi-Block Technique The solution space is split to a number of blocks, to simplify the grid generation and solution procedure. Each block is bounded between two adjacent blades in circumferential direction. In axial direction, each block is bounded between the adjacent cascade row and the boundary of the solution space. The technique is briefly described by Farhanieh et. al. [10] for a rotor- cascade. The required boundary condition is described in the next section.

3.5 Numerical Boundary Conditions The inflow and out flow boundary conditions were set for a transonic flow [9]. If our inflow is subsonic, the triple variables from outside at the inlet are P_t, T_t and the inflow angle, and if the outflow is subsonic, the P_s is computed from the upstream.

For the solid walls, the no-slip boundary condition is implemented.

For the upper and lower boundaries of both the rotor cascade and the stator cascade, the periodic boundary condition was used to give the circumferential continuity of the cascade. The values in fictitious cells of the lower boundary are set to be the same values as in the upper fictitious cells.

Each row of blades was split to multi zones for the multi-block technique and each block shares one or more boundaries with its surrounding blocks.

The common walls of the rotor and stator rows share their data in each time step with their adjacent wall boundary condition.

3.6 Grid Generation Each passage (between two blades) has an individual mesh, which is generated by mesh generator program using Partial Differential Equations (PDE) method. Clustering is available by related source terms as well as orthogonality. The mesh generated for each individual passage is considered as a single block, and the solver assembles them to prepare the complete area of solution by using the multi-block boundary condition.

3.7 Turbulence Modeling One of the groups of statistical turbulence models is the algebraic one or two-layer turbulence closure. These models can easily be implemented into a numerical algorithm,

but they require the determination of boundary layer parameters to calculate the eddy viscosity. In a complex flow such as the flow through a turbine or compressor cascade, the calculation of thickness of shear layer in a CFD code is difficult, because no realistic criterion can be found to define the edge of the boundary layer [10]. That is specially the case when flow separation exists within the domain.

An algebraic model, which is not written in terms of the boundary layer quantities and is very robust in separated regions, is the modified Baldwin-Lomax (BL) model [9]. He [6] has employed the BL model in a numerical investigation of Rotating-Stall inception in a multi-blade cascade flow in an axial compressor, with the possibility of having large-scale separated zones. Moreover, the comparison of other turbulence models such as κ-ε with BL model, done by Bohn et al. [11], shows the adequate assurance of using BL model in cascade problems. Regarding a large amount of memory required in multi-blades studies, the BL consumes the least memory and CPU time with respect to higher-order turbulence models. For the present work the BL model is employed.

In BL model the turbulent boundary layer is divided to inner and outer layers. The turbulent viscosity at inner layer is proposed by following relation [9]:

$$\mu_t = \rho l^2 |\omega| \tag{30}$$

which:

$$l = 0.41(1 - e^{-y^+/26})y \tag{31}$$

$$y^+ = \frac{u^* y}{\nu} \tag{32}$$

$$u_* = \sqrt{\frac{\tau_w}{\rho}} \tag{33}$$

and the vorticity is defined as following:

$$\omega = \frac{\partial u}{\partial y} - \frac{\partial v}{\partial x} \tag{34}$$

At the outer layer the turbulent viscosity is computed as follows:

$$\mu_t = \alpha \rho C_{CP} F_{Wake} F_{Kleb} \tag{35}$$

In which:

$$F_{Wake} = \min[y_{\max} G_{\max}, C_{Wake} y_{\max} \frac{(\Delta V)^2}{G_{\max}}] \tag{36}$$

$$G_{\max} = \max\left(\frac{l}{0.41}|\omega|\right) \tag{37}$$

$$F_{Kleb} = \left[1 + 5.5\left(\frac{C_{Kleb} y}{y_{\max}}\right)^6\right]^{-1} \tag{38}$$

$$C_{Kleb} = \frac{2}{3} - \frac{0.01312}{0.1724 - \beta^*} \tag{39}$$

$$\beta^* = \frac{y_{\max}}{u^*}\frac{\partial V}{\partial x} \tag{40}$$

$$C_{CP} = \frac{3 - 4C_{Kleb}}{2C_{Kleb}(2 - 3C_{Kleb} + {C_{Kleb}}^3)} \tag{41}$$

4. DISCUSSION OF RESULTS

4.1 Code Validations The performance of the described methodology is assessed via comparing the computed results to other approved dada.

The first test case is prepared for an incompressible flow over a flat plate, with the Mach number **M**=0.2. The Reynolds number is 10^6 and the transition point is set at the leading edge of the plate. This example demonstrates the performance of the solver with the employed turbulence model.

The good agreement of the results with the experimental results reported by Bohn et al., illustrated in Figure 2, shows that the grid resolution 200×80 used for the computational domain is sufficient to capture the boundary layer.

The second test study is prepared for the subsonic viscous flow over a NACA0012 airfoil.

The Reynolds number is set to 10^6 and the flow is turbulent. The inlet Mach number is set to 0.4 and the angle of attack is set to zero. Figure 3, shows the computed results, which are in a good agreement with experimental results reported by Fletcher [12].

This test case is prepared to examine the solver in viscous – turbulent flows with the existence of pressure gradients. This condition is a quite common in flows through a stage of an axial compressor. The grid resolution is the same as that in flat plate test case.

4.2 Unstable Flow Through the Compressor Stage The final study is prepared for flow through a compressor stage at the unstable point of operation of an axial compressor.

The geometrical characteristics of the blades in the stage are given in Table 1, and the flow characteristics in the stable and unstable operating conditions are given in Tables 2, and 3 respectively.

Figure 4, shows the stage as a multi-block zone, where each block is the passage between the upper and the lower surfaces of the two adjacent blades in each row. Each of the rotor and the stator rows contains 9 blades and, consequently, 10 passages. Five probes are located near the leading edge of blades in rotor row to indicate the required parameters.

The grid used in each passage is 75×41 with clustering and orthogonality near the solid walls. The total number of finite volume cells is to 61500 for the computational domain of the stage. Figure 5, shows an enlarged area of the grid used in the stage problem.

The numerical solution of the flow field in the stage shown in Figure 4, is started at the stable condition given in Table 2, After 3 revolutions of the rotor, the steady state stable solution was captured, and no instability effect were detected. The steady solution was chosen as a basis to study the unstable condition and at this point the time was set to zero. The inlet flow angle, the axial velocity and the exit pressure were changed to the values given in Table 3, at the same rotating speed chosen in stable operating condition. The axial velocity traces obtained from the probes shown in Figure 4, can be illustrated with respect to dimensionless time. To distinguish the velocity traces, the curves are shifted by a constant value. Evidently, the axial velocity traces show a cyclic behavior of the flow and the five velocity traces have phase differences, the period of the cycles are 83% of the period of rotation. The two times t_A and t_B were set for the minimum

TABLE 1. Geometrical Characteristics of the Stage.

Stagger angel of rotor blades	55°
Stagger angel of stator blades	35°
Rotor blade profile	NACA65-(A_{10})
Stator blade profile	NACA65-(A_{10})
Solidity	1.0
Gap in percent of chord	37%

TABLE 2. The Stable Condition.

r_h/r_t	0.6
R	0.56
P_{in}	100000 Pa
T_{in}	300 K°
P_{exit}/P_{in}	1.02589
β_1	62°
ψ	0.28
ϕ	0.4
V_{xin}	36 m/s
M_{in}	0.223
U_r	90 m/s
RPM	1240
Pexit/Pin	1.02989
β1	72°
Vxin	22 m/s
ϕ	0.24
RPM	1240

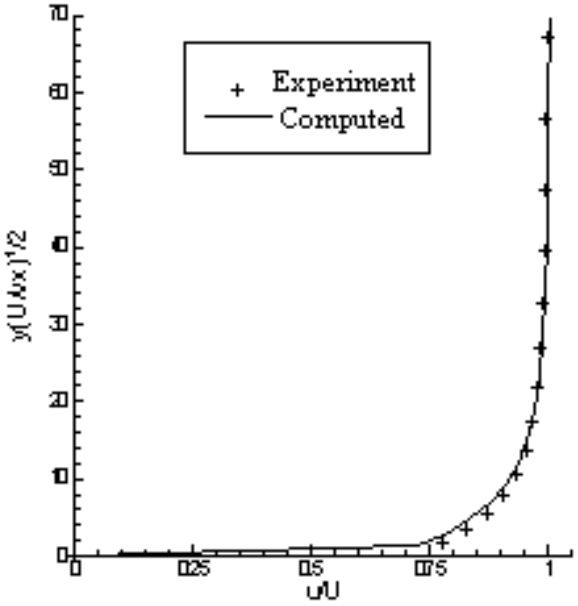

Figure 2. Comparing the computed velocity profile for flat plate with the experimental profile at 68% of plate length, from the leading edge of the flat plate.

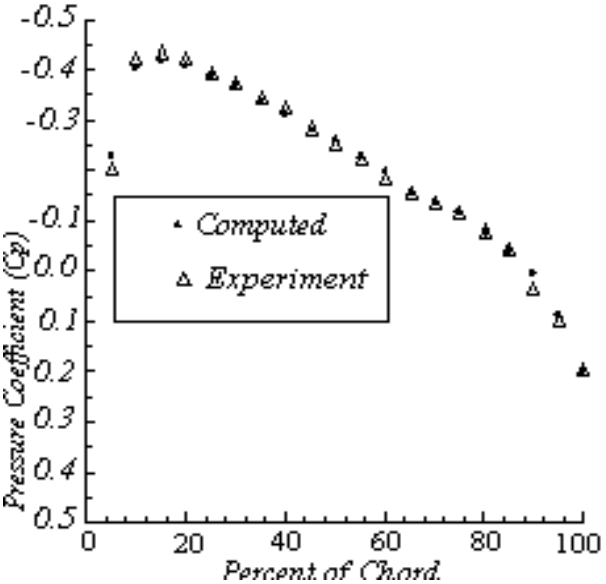

Figure 3. Computed and experimental Pressure coefficients over a semi NACA0012 airfoil. Mach number is 0.4 and Reynolds Number is 10^6.

TABLE 3. The Unstable Condition.

P_{exit}/Pin	1.02989
β_1	72°
Vx_{in}	22 m/s
ϕ	0.24
RPM	1240

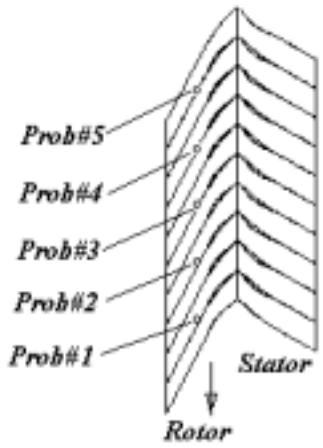

Figure 4. Multi-block geometry of the Compressor stage.

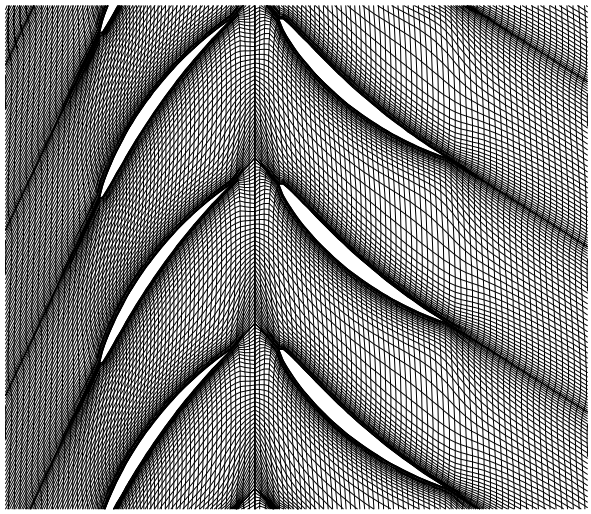

Figure 5. The enlarged area of the mesh generated for the stage.

and maximum peaks of the velocity trace of the first probe. To study the reason of the cyclic

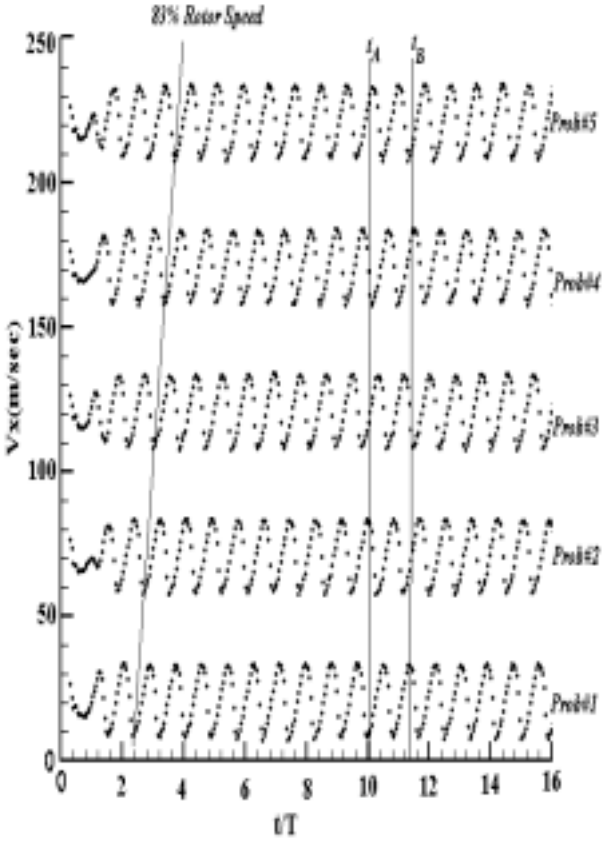

Figure 6. Axial Velocity traces with respect to rotor revolutions.

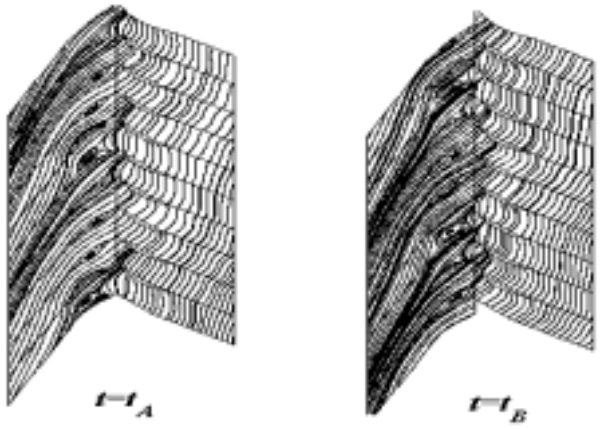

Figure 7. Unstable Streamlines at the relative frame.

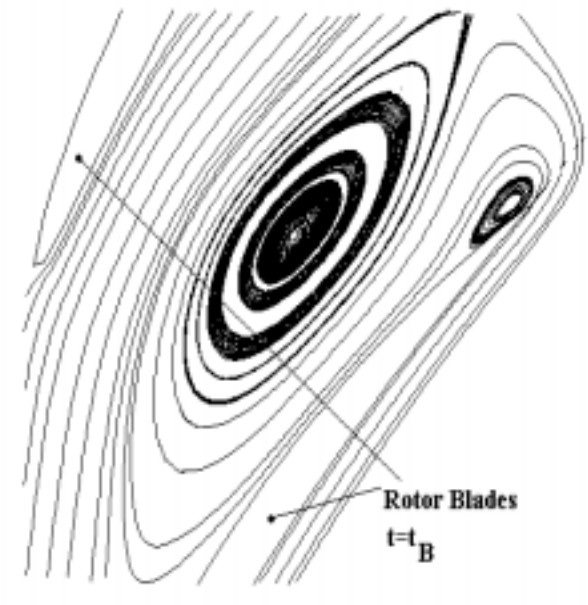

Figure 8. The Deep Cell in rotor blades at $t = t_B$.

behavior of the traces, the streamlines of the stage in relative frame are shown in Figures 7, for the times t_A and t_B. The streamlines show that in time t_A, nine of ten passages contain instability vortices, two of them in the first and sixth passages (from the bottom) are greater than the others and it seems that they are growing in size. It is also evident that the flow entering the second passage (passing over the first probe) in time t_A, is deviated from its entering angle shown in time t_B. This may cause the reduction of the axial velocity at the time t_A, and the increase of it in t_B on the first probe. The Figure 6, shows the growth, the diffusion and the movement of the vortices.

In time t_A there are two growing cells in the first and sixth passages. At t_B, the cells are grown and they are moved to the fourth and ninth passages. The studies show that the diffusion, growing and the movement of the vortices were repeated and this can cause the cyclic behavior of the velocity traces.

The cyclic behavior of the velocity traces is similar to the mass flow rate traces of the in viscid solutions reported by Saxer et al. [8]. The velocity traces reported by He [6] also show that a fully developed rotating stall has a constant frequency.

Figure 9. Pressure Contours for the deep cell at $t=t_B$.

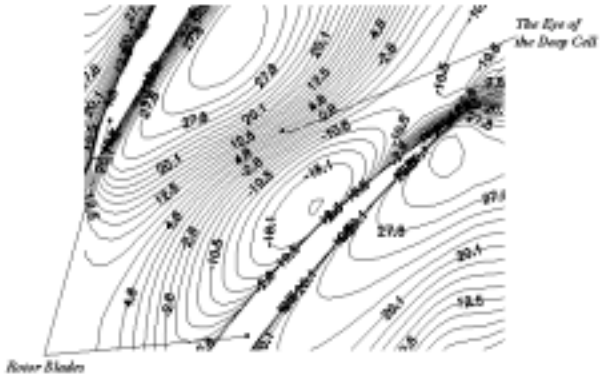

Figure 10. Axial velocity contours for the deep cell in relative frame at $t= t_B$

This frequency depends on the noises of the input pressure field. In this work, the input pressure field is free of any exciting frequency, and the rotating stall inception becomes form the reduction of the mass flow rate and exceeding of the exit pressure, which moves the operating point of the compressor stage to the instability region of the compressor map.

The generation, growth and the diffusion of the vortices in a rotating stall indicates that the effect of a vortex in a rotating stall may differ from that in a simple separated area.

To study the instability vortices, a more detailed investigation is prepared for the deep cells captured in time t_B. Figure 7, shows the deep cell in the relative frame and Figures 8 and 9 show, respectively, the pressure and the axial velocity contours for the deep cell. Figure 8, shows that the pressure value is minimum in the eye of the cell and toward the downstream there is an adverse pressure gradient. Figure 9, shows that the axial velocity becomes negative near the cell, which is in agreement with those reported by Saxer et al. [8].

5. CONCLUSION

A multi-blocks 2-D solver was developed to investigate the viscous approaches in turbomachinery through-flow problems. The viscous-turbulent flow over a flat plate and the flow over a NACA0012 airfoil were considered, to validate the solver and the required grid resolution in viscous-turbulent flows. The test cases of NACA0012 demonstrate the grid performance of the solver.

The rotating stall effect was captured for the flow through the stage of an axial compressor by varying the operating point to the unstable condition. The results show that this mode of rotating stall may have a constant frequency in axial velocity traces and this depends on the cyclic configuration of the moving cells. The results have nearly the same characteristics as with these reported in previous numerical works.

Considering separated flow over a single airfoil in a high angle of attack and the results of the present work, it may be concluded that the moving, growing and the diffusion of an instability vortex in the cascade flow are completely different from those of a separated vortex on an airfoil with a high angle of attack. It may be concluded that the multi-blade cascade geometry, the adverse pressure gradient, and the reduction in mass flow rate which increases of the inlet angle of attack in a constant rotating speed, may be the main causes of starting the rotating stall effect.

6. NOMENCLATURE

ρ	density

ℓ	limiter function
$\mathbf{Q}$	unknown vector
$\tilde{u}$	averaged u at cell boundary
$\hat{\delta}^+, \overline{\delta}^+$	limited slopes
$\overline{\mathbf{F}}$	transformed inviscid flux vector in η direction
$\overline{\mathbf{E}}$	transformed inviscid flux vector in ξ direction
$\overline{\mathbf{Q}}$	transformed of **Q**
$\overline{\mathbf{E}}_v$	transformed viscous vector flux vector in ξ direction
$\overline{\mathbf{F}}_v$	transformed viscous flux vector in η direction
v	x-direction component of velocity vector
u	x-direction component of velocity vector and a abitrary parameter.
ϕ	flow coefficient
ψ	load coefficient
β1	inlet angle of relative
$\mathbf{\Lambda_g}$	diagonal matrix with its elements being the eigen values
$\lambda i^{\pm}$	eigen values of $\mathbf{A^{\pm}}$
λi	eigen values of **A**
μt	turbulent viscosity
∂V	bounding surface of volume V
ΔV	Maximun velocity difference in normal direction
ξ_x	partial of ξ with respect to x
η_x	partial of η with respect to x
ξ_y	partial of ξ with respect to y
η_y	partial of η with respect to y
A	Jacobian matrix for $\overline{\mathbf{E}}$
$\mathbf{A^{\pm}}$	decomposed matrix of **A**
μ	absolute viscosity
$\mathbf{A_v}$	Jacobian matrix for $\overline{\mathbf{E}}_v$
B	Jacobian matrix for $\overline{\mathbf{F}}$
$\mathbf{B_v}$	Jacobian matrix for $\overline{\mathbf{F}}_v$
C	velocity of sound
E	total energy
F	overal flux vector
$\mathbf{F_E}$	inviscid flux vector
$\mathbf{F_v}$	viscous flux vector
g(A)	any matrix having the right and left eigenvectors
H	total enthalpy
ξ	horizontal axis of transformed coordinate
I	unit tensor
i	cell index in ξ direction
j	cell index in η direction
J	Jacobian transformation
k	$k = \frac{C_p}{C_v}$
L	eigenvector matrix of **A**
$\mathbf{L^{-1}}$	Inverse matrix of **L**
$\boldsymbol{M}$	Mach number
M_{in}	Inlet Mach number
$\boldsymbol{M_n}$	Mach number in **n** direction
n	normal vector of **A**
P	thermodynamic pressure
P_{exit}	down stream pressure
P_{in}	inlet pressure
P_s	static pressure
P_t	total pressure
q	Heat flux
R	constant of ideal gas and the reaction degree
RPM	Roation velocity of the Rotor
ω	slope averaging parameter
σ	stress tensor
t	time in physical coordinate
τ	time in transformed coordinate
Tin	inlet temperature
T_s	static temperature
T_s	static temperature
T_s	static temperature
T_t	total temperature
U	velocity vector
U_r	Linear rotation velocity of the Rotor.
V	inviscid velocity in η direction
V	volume velocity
η	vertical axis of transformed coordinate
V_x	Axial velocity in stage
V_{xin}	inlet axial velocity
x	vetical axis of Cartesian coordinate
x_ξ	partial of x with respect to ξ
x_η	partial of x with respect to η
y	horizontal axis of Cartesian

	coordinate
y_ξ	partial of y with respect to ξ
y_η	partial of y with respect to η
y_{max}	The point of maximum velocity in normal direction

7. REFERENCES

1. Inue, M., Kuroumaru, M., Tanino, T. and Furukawa, M., "Propagation of Multiple Short-Length-Scale Stall Cells in an Axial Compressor Rotor", ***ASME Journal of Turbomachinery*****,** Vol. 122, (2000), 45-53.
2. Day, I. J., Breuer, T., Escuret, J., Cherrett, M. and Wilson, A., "Stall Inception and the Prospects for Active Control in Four High-Speed Compressors", ***ASME Journal of Turbomachinery*****,** Vol. 121, (1999), 18-27.
3. Silowski, P. D., "Measurements of Rotor Stalling in a Matched and a Mismatched Multistage Compressor", ***GTL Report, Gas Turbine Laboratory, Massachusetts Institute of Technology***, No. 221, (1995).
4. Sisto, F., Wu, W., Thangam, S. and Jonnavithula, S., "Computational Aerodynamics of Oscillating Cascade with Evolution of Rotating Stall", ***AIAA Journal***, Vol. 27, (1989), 462-471.
5. Jonnavithula, S., Thangam, S. and Sisto, F., "Computational and Experimental Study of Stall Propagation in Axial Compressors", ***AIAA Journal***, Vol. 28, (1990), 1945-1952.
6. He L., "Computational Study of Rotating-Stall Inception in Axial Compressors," ***Journal of Propulsion and Power***, Vol. 13, (1997), 31-38.
7. Outa, E., Kato, D. and Chiba, K., "A N-S Simulation of Stall Cell Behavior in a 2-D Compressor Rotor-Stator System at Various Load", ***ASME Paper***, No. 94-GT-257. (1994).
8. Saxer-Flelici, H. M., Saxer, A. P., Inderbitzen, A., Gyarmathy, G., "Prediction and Measurement of Rotating Stall Cell in an Axial Compressor", ***ASME Journal of Turbomachinery***, Vol.121, (1999), 365-375.
9. Hoffman, K. A., Chiang, S. T., "Computational Fluid Dynamics for Engineers", A Publication of Engineering Education System™", Wichita, Kansas, 67208-1078, USA, ISBN 0-9623731-7-6, (1993).
10. Farhanieh, B., Amanifard, N. and Ghorbanian, K., "Numerical Investigation on Compressible Flow Characteristics in Axial Compressors Using a Multi-Block Finite-Volume Scheme", ***International Journal of Engineering***, Vol. 15, No. 1, (2002), 91-104.
11. Bohn D. and Emunds R., "A Navier-Stokes Computer Code for Theoretical Investigations on the Application of Various Turbulence Models for Flow Prediction Along Turbine Blades", ***Proceeding of the International Gas Turbine and Aero-engine Congress and Exposition***, Houston, Texas, 95-GT-90, (June 5-8,1995).
12. Fletcher, C. A. J., "Computational Techniques for Fluid Dynamics 2", Springer-Verlag, ISBN 0-387-18759-6, (1991).